Chapter 11
Tollmien-Schlichting Waves Artificially Inserted in Boundary Layer by Harmonic Point Source

Victor Barcelos Victorino, Christian Salaro Bresci, Matheus Maia Beraldo, and Marcello Augusto Faraco de Medeiros

Abstract The present work experimentally investigates the spatial evolution of controlled artificial disturbances inserted by a harmonic point source in a Blasius boundary layer over a flat plate. A small hole of 0.80 mm diameter is responsible to introduce a blowing and suction flow inside the boundary layer induced by an embedded loudspeaker. The model employed consists of a plexiglass plate with an 1800 mm chord, 1000 mm span, and 10 mm thickness, vertically assembled inside the test section of the Low Acoustic Noise and Turbulence (LANT) wind tunnel at EESC-USP. Aluminum leading edge, flap, and tab were attached to the model in order to promote a practically constant pressure distribution. Hot-Wire Anemometry was carried to measure base flow, turbulence level, and Tollmien-Schlichting profiles. Good agreement with Blasius was obtained in at least a 300 mm span range, on two different streamwise positions. Tollmien-Schlichting eigenfunction profiles were measured for different positions in a chordwise direction. The amplification region matches that predicted by Linear Stability Theory. Through spectral analysis, it was possible to identify the presence of fundamental and first harmonic oscillation, which led to the conclusion that the flow conditions corresponded to a weakly non-linear regime.

Keywords Tollmien-Schlichting wave · Harmonic point source · Transition in boundary layer · Flow Instability

11.1 Introduction

Flow instabilities and the onset of turbulence in the boundary layer are characterized by complex nature and chaotic motion. Such dynamics arise from, among several mechanisms, interactions of non-linear effects on oscillations present in

V. B. Victorino · C. S. Bresci · M. M. Beraldo · M. A. F. de Medeiros (✉)
USP, EESC, São Paulo, SAA 13566-590, Brazil
e-mail: marcello@sc.usp.br

V. B. Victorino
e-mail: barcelos.victorino@usp.br

H. F. Meier et al. (eds.), *Advances in Turbulence*, ABCM Series on Mechanical Sciences and Engineering, https://doi.org/10.1007/978-3-031-25990-6_11

the flow. Once a turbulent regime is reached, time-dependent motion promotes mass, momentum, and energy transference and as a consequence, losses become strongly affected. Therefore, engineering and physical sciences search for better understanding of the process.

First experimental evidence of flow turbulence was reported by Reynolds (1883). Following, Tollmien (1928) and Schlichting (1933) worked on the development of the Linear Stability Theory (LST), which is based on the stability of viscous laminar Blasius boundary layer to small amplitude disturbances. Nevertheless the validation of the LST was achieved only after experimental evidences was obtained by Schubauer (1948). The theory is derived from linearized Navier-Stokes equations (LNSE) applied on parallel flows, e.g., two-dimensional boundary layer. Variables are decomposed into time-invariant component (base flow) and time-dependent small amplitude harmonic oscillation. Non-linear terms are neglected, because it is assumed that the amplitude is small compared to the base flow magnitude. After manipulation and the application of normal modes analysis, the equation

$$(\alpha U - \omega)(\phi'' - \alpha^2\phi) - \alpha U''\phi = -\frac{i}{Re_{\delta^*}}(\phi'''' - 2\alpha^2\phi'' + \alpha^4\phi) \tag{1}$$

commonly referred to as Orr-Sommerfeld equation can be treated as an eigenvalue problem.

Originally, the LST treated the problem as temporal and once specified α and Re_{δ^*}, the complex eigenvalue, ω, is the solution. This variable represents temporal frequency and its imaginary part $\Im(\omega)$, called amplification factor. It determines whether the associated spatial wavenumber, α, at a specific Re_{δ^*} is stable ($\Im(\omega) < 0$) or unstable ($\Im(\omega) > 0$). The eigenfunction, $\phi(y)$, describes the amplitude profile across the wall-normal direction (y), and the instability wave characterized by these parameters is named Tollmien-Schlichting (T-S) wave. After several calculations for different combinations of parameters, the instability locus can be mapped and it is usually plotted by means of the neutral stability curve diagram. The maximum Reynolds number based on displacement thickness, Re_{δ^*}, for which no amplification occurs is called critical Reynolds (Re_{crit}) and two branches bound the instability region. Such boundaries correspond to a region where $\Im(\omega) = 0$. It is important to point out the fact that the perturbations artificially imposed in the boundary layer at a fixed streamwise position consist of a spatial problem. Later, Gaster (1962) demonstrated through the Cauchy-Riemann relations that the spatial growth is related to temporal growth by the group velocity, $c_g = d\omega/d\alpha$.

Schubauer (1948) pointed out that the study of T-S waves produced by controlled artificial disturbances could be more beneficial than under natural circumstances, e.g., free-stream turbulence. Perturbation source devices of various kinds were explored and the vibrating ribbon was the most appropriate accordingly to the authors. Klebanoff et al. (1962) also performed experiments through this technique and remarkable contributions were achieved about the three-dimensional nature of T-S wave, characterized by spanwise pattern in wave amplitude. The authors stated that

the actual breakdown of wave motion to turbulence occurs as a consequence of non-linear three-dimensional effects that lead to secondary instabilities by the formation of hairpin eddies. Afterward, this regime was named the K-type transition.

In addition, another laminar breakdown regime was observed by Kachanov et al. (1977), also reported by Kachanov and Levchenko (1984) and Kachanov (1994). In this type of transition, no turbulent spikes of unsteady velocity records were observed, as opposite to Schubauer (1948). The spectral analysis of this transition process leads to a subdivision of four stages. Initially, weakly linear development occurred as well as the growth of fundamental frequency harmonics of the perturbation imposed over the flow. The second stage is marked by the growth attenuation of these components and the appearance of low-frequency and sub-harmonic components in the spectrum. Subsequently, three-dimensional effects were reported followed by interaction among the low-frequency pulsation, fundamental mode, and its harmonics. Lastly, the process presents attenuation of harmonics and laminar breakdown. This kind of transition driven by three-dimensional resonance interactions was called N-type transition.

Gaster (1990) carried out experiments employing a harmonic point source to stimulate T-S waves in a Blasius boundary layer. The device selected as the source was a small loudspeaker buried in the plate. Transmission of disturbance to boundary layer flow was due to ring of small holes of 0.30 mm diameter in which a blowing and suction flow was induced by the loudspeaker. Three types of input signal were investigated: a periodic monochromatic sinusoidal wavetrain, a controlled broadband noise, with low amplitude relative to sinusoidal signal, and a composition of both. Despite no turbulence being reached through the regime employed, results exhibited a spectrum similar to those obtained by Kachanov and Levchenko (1984). The author concluded that large amplitude Tollmien-Schlichting waves are unstable to weak excitations at a subharmonic frequency and its multiples. The rate of amplification of the secondary motion was proportional to the square of the fundamental driving signal as expected based on weakly non-linear theory.

The non-linear evolution of a wavetrain emanating from a point source was also experimentally investigated by Medeiros (2004). The disturbance amplitude employed was sufficient to promote a weakly non-linear behavior. The results exhibited a three-dimensional mean flow distortion in the form of longitudinal streaks. Two distinct stages of the non-linear regime were reported. The first was characterized by a low spanwise wavenumber apparently associated with a pair of counter-rotating streamwise vortical regions. It was found that the phenomenon arise from the interaction between spanwise and wall-normal modes. The second stage presented more streaks and a higher spanwise wavenumber. The streamwise location of this stage onset was not influenced by the input amplitude, and appeared to be associated with the second branch of the neutral stability diagram.

Present work concerns the experimental study of the development of artificial Tollmien-Schlichting waves in a Blasius boundary layer. The disturbance source device employed was a small loudspeaker, like that used by Gaster (1990) and Medeiros (2004). Such disturbance is characterized by three-dimensional nature and depending on input amplitude, non-linear effects can become significant. The

eigenfunction profile was measured and spectral analysis was employed. An attempt to identify some aspects related to previously cited references was carried out and LST calculations were applied in order to verify whether the experimental results match the predictions by theory.

11.2 Experimental Setup

The current work experiments were performed in the Low Acoustic Noise and Turbulence wind tunnel (LANT) located at EESC-USP. Such facility provides a good quality flow for transition study purposes, the free-stream turbulence intensity measured with an empty test section is 0.05%. The test section possesses a squared cross-sectional area of 1.00 m^2 and a length of 3.00 m. Figure 1 exhibits the floor plan of the wind tunnel facility, where the aforementioned devices are highlighted by colored schemes.

The model consists of a plexiglass flat plate (element number 2 in Fig. 2) with 1800 mm chordwise length, 1000 mm span, and 10 mm thickness, vertically installed inside the test section. An asymmetrical modified super-ellipse leading edge (element number 1 in Fig. 2) is attached at the frontal region of the plate, while at the trailing edge, a flap and tab set (elements number 3 and 4, respectively, in Fig. 2) are installed, all of them made of aluminum. This last apparatus is used to ensure a good pressure distribution, which is no significant pressure gradient along the experiment envelope region, and to position the stagnation line slightly at the work-side. The leading edge geometry was designed to prevent suction peak on work-side surface, and to promote reduced length where the pressure settles after the stagnation point (Hanson et al. 2012). The pressure distribution was measured through static pressure taps

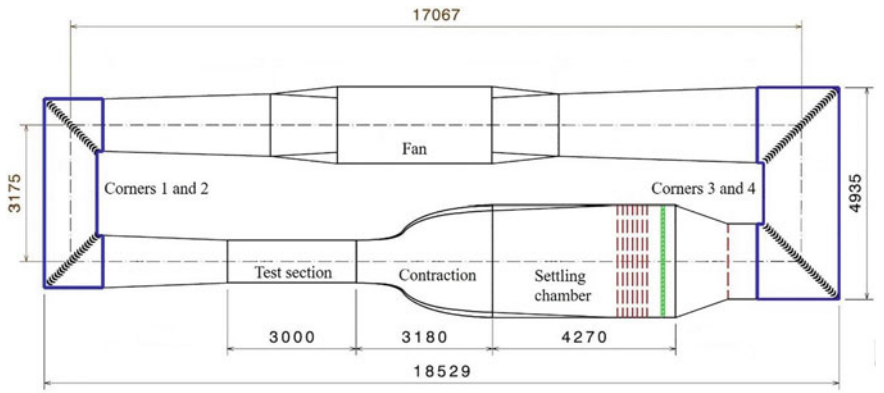

Fig. 1 Floor plan of LANT wind tunnel. The black C-shaped lines arrays indicate the corning vanes, blue boxes, the region coated by acoustic absorber foam, red dashed lines, the screens and green hatched strip, the honeycomb ducts. Air flows in clockwise direction. Dimensions in millimeters

distributed along the model and attached to an inclined U-tube manometer bank. Figure 2 exhibits the isometric view of the flat plate model, Fig. 3 displays the leading edge super-elliptical profile.

Located over the centerline, 200 mm distant from the flat plate leading edge, there is a small through-hole with 0.80 mm diameter connected to a cavity inside the plate. A loudspeaker was buried in the cavity and was responsible for the excitation of a controlled disturbance into the boundary layer flow. The loudspeaker diaphragm was flush to the entrance of the small diameter duct, and when driven by a signal input, vibration motion induced a blowing and suction flow. This flow was responsible for introducing a harmonic point source perturbation. The input signal was transmitted by an Agilent 33500B function generator. A sine-like monochromatic wave with 200 Hz frequency and 250 mV amplitude was chosen as input.

Hot-Wire Anemometry was the technique selected for velocity measurements. The constant temperature anemometer circuit model DISA 55D01 includes a DANTEC 55P05 tungsten probe with a filament diameter of 5 μm and length of 1 mm. The output signal was branched and transmitted to two acquisition devices. The first consists of 16-bit resolution National Instruments (NI) DAQ USB-6002 module, and

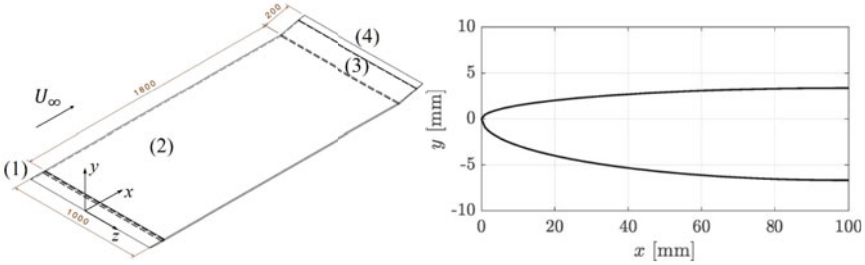

(a) Model. (b) Leading edge.

Fig. 2 Isometric view of model and asymmetrical leading edge profile. Dimensions in millimeters

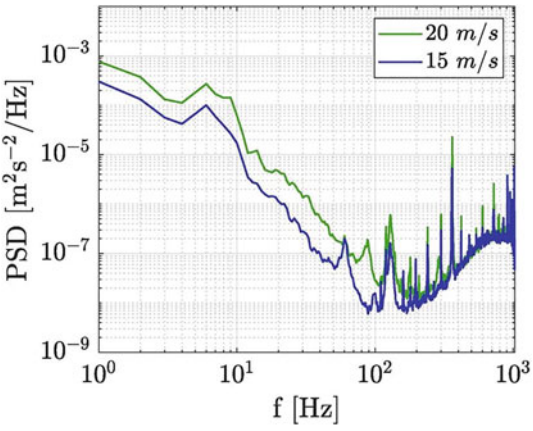

Fig. 3 Power spectral density of unsteady free-stream velocity component

it was responsible for recording the DC voltage component. The second instrument, responsible for acquiring AC voltage component signal, was an acquisition board NI 4498, with 24-bit resolution and 114 dB dynamic range, connected to a NI PXI-1042Q chassis. Conditioning and manipulation of the signal were performed by MATLAB scripts. The position of the probe inside the test section was controlled by an in-house traverse mechanism. A calibration operation to convert voltage in velocity was done in situ. A script was able to fit the parameter values, through King's Law correlation between the velocity, measured by a static pitot tube placed inside the test section, and the output voltage of the anemometer. Environment conditions, such as atmospheric pressure, ambient and flow temperatures, were also employed. The traverse position, as well as data acquisition, were controlled by computer routines. The distance from the wall was obtained using the Blasius profiles as a reference.

11.3 Results

11.3.1 Preliminary Results

Preliminary experiments were conducted for base flow verification. Turbulence intensity was measured at position x = 400 mm, 150 mm distant from the flat plate work-side surface over the centerline. The signal was acquired at a rate of 2048 samples/s during 100 s, for two different free-stream velocities, $U_\infty = 15$ ms^{-1} and $U_\infty = 20$ ms^{-1}. Two techniques were employed for signal conditioning and turbulence evaluation, respectively. Firstly, Welch's method (Cryer et al. 2010) was implemented in order to estimate the power spectral density (PSD). Such method reduces frequency resolution to improve the signal-to-noise ratio by reshaping the raw signal into 100 blocks, each one with 1 s time length, followed by the ensemble average of the PSD. The other technique, provided by Lindgren (2002), consists of applying a dynamic filter with a cut-off frequency given by $f_c = U_\infty/\lambda_c$. The parameter $\lambda_c = 2$ m was set based on twice the maximum reference length of the test section side. Turbulence intensity was calculated by $Tu = u_{rms}/U_\infty[\%]$ and root-mean-square (RMS) was calculated by the square root of PSD sum along the interval given by cut-off and Nyquist frequencies. Figure 3 shows the PSD of free-stream unsteady velocity component. The spectrum behaves as expected. It is possible to note high energy at low-frequency range of approximately 4–10 Hz, typical of closed-circuit wind tunnels and a region with energy decay in the range of 0–200 Hz. A smooth peak related to traverse vibration occurs around 140 Hz, however, such component did not interfere with the results. Sharp peaks associated with power line utility frequency ($f_{pl} = 60$ Hz) and its harmonics ($n \cdot f_{pl}; n = 1, 2, 3 \ldots$) are also noticed. For both velocities, the turbulence intensity measured was $Tu = 0.10\%$, which is suitable for current work.

The mean velocity boundary layer profile was measured and compared to Blasius' theory. Two sets of profiles were taken in two distinct streamwise positions, x =

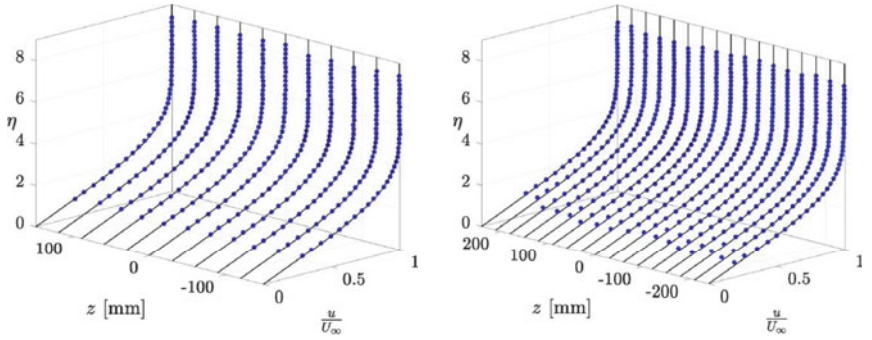

(a) x = 200 mm. (b) x = 900 mm.

Fig. 4 Experimental mean velocity profile (blue dots) along span in comparison with Blasius (black solid lines) for two different chordwise positions

200 mm and x = 900 mm, both with the discretization of 30 mm, covering a span (z-axis) of 300 mm and 480 mm, respectively. The free-stream velocity was set constant near the velocity employed for T-S experiments (≈17 ms^{-1}). The discretization in the wall-normal direction was set to 0.10 mm, at x = 200 mm, and 0.20 mm, at x = 900 mm. Wall distance of the measurement point closest to the model surface was estimated assuming the Blasius profile. Each profile was normalized by the boundary layer edge velocity, calculated by the mean velocity of the five most distant points from the model surface. The wall-normal direction (y-axis) is represented by the similarity parameter $\eta = y\sqrt{(U_\infty/\nu x)}$. Kinematic viscosity, $\nu = 1.76\times10^{-5}$ m^2s^{-1}, was calculated given mean flow temperature, and airflow density calculated by ideal gas relation for environmental conditions measured, $\rho = p_{atm}/RT_\infty$. Figure 4 shows the comparison between theoretical Blasius and experimental profiles. It is noted a good agreement with Blasius and high uniformity of boundary layer across the span covered.

11.3.2 Tollmien-Schlichting Waves

Six Tollmien-Schlichting amplitude profiles were measured in a streamwise (x-axis) range of 500–1000 mm, spaced by 100 mm. The free-stream velocity was set constant at $U_\infty = 17.3\,ms^{-1}$. The unsteady velocity records were taken along 31 s for each measurement point, with a sampling rate of 2000 samples/s. Welch's method was employed to increase the signal-to-noise ratio, by segmenting the raw signal into 35 blocks and taking the ensemble average to estimate the PSD. The profile amplitude of u' was given by the RMS of the unsteady record, which was calculated by the square root of PSD summed over a narrow interval centered at 200 Hz. Such range covered a $\pm2\Delta f$ wide span, where $\Delta f \approx 1.15$ Hz is the frequency resolution of the reshaped signal. The sum interval was chosen based on the PSD analysis, it was

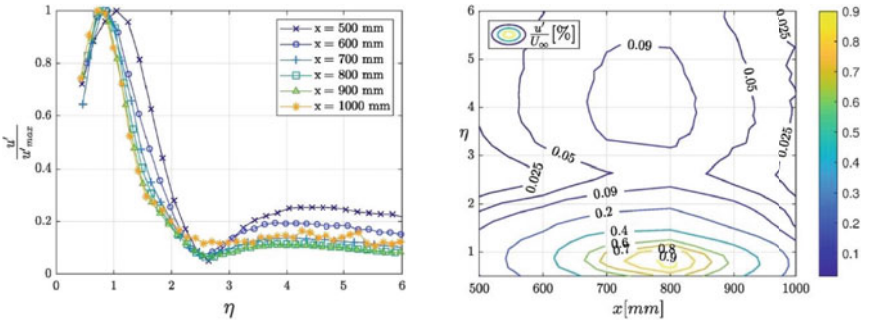

(a) Normalized TS profiles for different chordwise position.

(b) Contour of u'/U_∞ [%] amplitude on $x\eta$ plane.

Fig. 5 Experimentally measured Tollmien-Schlichting waves

necessary to include possible power leakage arising from Welch's method, although it should not include undesired energy of other frequency components.

Figure 5 (a) exhibits normalized profile for each x position, Fig. 5 (b) displays contours of percentage amplitude relative to free-stream velocity ($u'/U_\infty[\%]$) for the $x\eta$ plane. Analysis of Fig. 6 indicates that the T-S peak location becomes sharper as it evolves across a streamwise direction, which is expected since the non-normalized amplitude increases downstream within the instability region. Around the local maximum next to $\eta \approx 4$, one can note a decrease trend of the outer peak across the x-axis, and after the T-S reaches stability at x > 800 mm, a distortion seems to appear in amplitude profile. This is showed also in Fig. 5b.

The T-S inner peak spectrum was also investigated and it is shown in Fig. 6 by the dark blue solid lines. Several characteristics consistent with the flow instability are seen. Firstly, a bell-shaped amplitude value within a frequency band is present in the PSD plot of almost all x positions covered. This behavior is expected, since it exhibits the disturbances amplification of the unstable frequencies, which naturally arise inside the boundary layer. The light blue and yellow dash-dot lines displayed in Fig. 6 locate the dimensional frequency of branches I and II of the neutral curve stability diagram, respectively. Such values were obtained by in-house codes that solve Linear Stability Theory (LST) problem. In the range of 500 mm $\leq$ x $\leq$ 800 mm, the branch II frequency practically coincides with the maximum of those bell-shaped bulges, which is expected accordingly to LST. However, once the dominant forced perturbation with a frequency of 200 Hz is no longer unstable, the behavior of the remaining unstable frequencies apparently changes and the most amplified frequency appears close to the center of the unstable region delimited by the branches, around 100 Hz. A sharp peak at 200 Hz is highlighted by the green dashed line in Fig. 6a–f. As such frequency remains within the range of unstable frequencies, disturbance growth occurs.

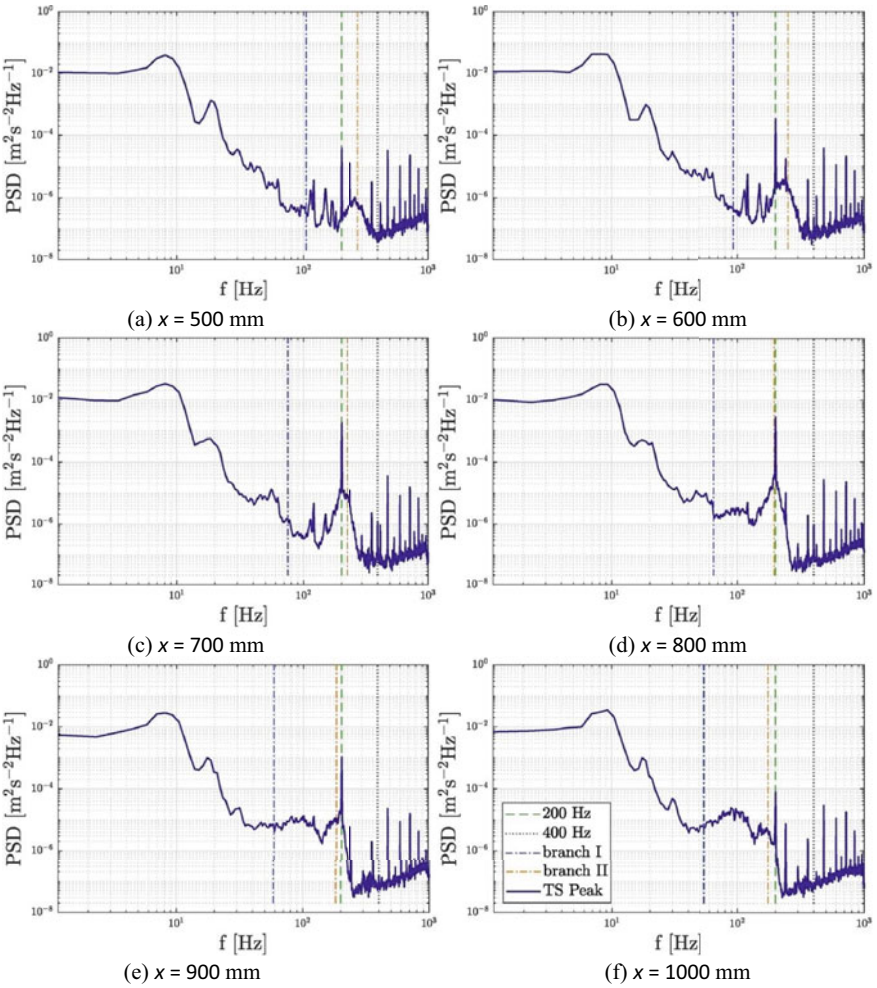

Fig. 6 Power spectral density of T-S peak along the streamwise direction x

11.4 Concluding Remarks

Tollmien-Schlichting waves were artificially excited by a harmonic point source. The base flow over a flat plate with a virtual zero pressure gradient was characterized, including the free-stream turbulence intensity. A good agreement with Blasius was reached and a suitable level of turbulence was obtained. It was possible to measure the eigenfunction amplitude profile. Amplitude growth occurred inside the unstable region predicted by LST, as well as damping at positions downstream of branch II of the neutral curve. By analysis of PSD corresponding to the T-S peak location, it was possible to identify some aspects provided by Gaster (1990) and Kachanov et al.

(1977). Among which was possible to notice the presence of the first harmonic of fundamental disturbance (400 Hz). This component should not be amplified, once it is located in a stable locus of the stability diagram, however, growth was observed. Apparently, this component arises from non-linear interactions and its amplitude is related to the amplitude of fundamental disturbance (200 Hz). Low frequencies around the sub-harmonic (100 Hz) also presented amplification at downstream positions. As pointed out by Gaster (1990), this fact could be associated with the instability of relatively large amplitude T-S waves to small perturbations within frequencies close to sub-harmonic components.

Acknowledgements V.B.V. was funded by CNPq/Brazil, grant #134335/2018-0. C.S.B. was funded by CAPES/Brazil, under the CAPES/PROAP Social Demand program. M.M.B. was funded by CAPES/Brazil, grant #88882.379172/2019-1. M.A.F.M. thanks the National Council for Scientific and Technological Development (CNPq/Brazil) for grants 307956/2019-9 and the US Air Force Office of Scientific Research (AFOSR) for grant FA9550-18-1-0112, managed by Dr. Geoff Andersen from SOARD. The LANT wind-tunnel financial support was provided by FINEP/Brazil, grant #01.09.0334.04. The authors also thank FAPESP/Brazil for grant 2019/15366-7.

References

Cryer JD, Bendat JS, Piersol AG (2010) Random data—analysis and measurement procedures, 4th edn, vol 82. John Wiley & Sons, Inc. ISBN 9780470248775. https://doi.org/10.2307/2289430

Gaster M (1990) The nonlinear phase of wave growth leading to chaos and breakdown to turbulence in a boundary layer as an example of an open system. Proc R Soc Lond Ser A Math Phys Sci 430(1878):3–24. ISSN 0962-8444. https://doi.org/10.1098/rspa.1990.0078

Gaster M (1962) A note on the relation between temporally-increasing and spatially-increasing disturbances in hydrodynamic stability. J Fluid Mech 14(2):222–224. ISSN 14697645. https://doi.org/10.1017/S0022112062001184

Hanson RE, Buckley HP, Lavoie P (2012) Aerodynamic optimization of the flat-plate leading edge for experimental studies of laminar and transitional boundary layers. Exp Fluids 53(4):863–871. https://doi.org/10.1007/s00348-012-1324-2

Kachanov YS (1994) Physical mechanisms of laminar-boundary-layer transition. Annu Rev Fluid Mech 26:411–482

Kachanov YS, Kozlov VV, Levchenko VY (1977) Nonlinear development of a wave in a boundary layer. Fluid Dyn 12(3):383–390. ISSN 15738507. https://doi.org/10.1007/BF01050568

Kachanov YS, Levchenko VY (1984) The resonant interaction of disturbances at laminar-turbulent transition in a boundary layer. J Fluid Mech 138(1984):209–247. ISSN 14697645. https://doi.org/10.1017/S0022112084000100

Klebanoff PS, Tidstrom KD, Sargent LM (1962) The three-dimensional nature of boundary-layer instability. J Fluid Mech 12(1):1–34. ISSN 14697645. https://doi.org/10.1017/S0022112062000014

Lindgren B, Johansson AV (2002) Evaluation of the flow quality in the mtl wind-tunnel. Technical report, Royal Institute of Technology Department of Mechanics, SE-100 44 Stockholm, Swede. https://www.mech.kth.se/oso/papers/MTL_techrep.pdf

Medeiros MAF (2004) The nonlinear evolution of a wavetrain emanating from a point source in a boundary layer. J Fluid Mech 508:287–317. https://doi.org/10.1017/S0022112004009188

Reynolds O (1883) An experimental investigation of the circumstances which determine whether the motion of water shall be direct or sinuous, and of the law of resistance in parallel channels. Philos Trans R Soc Lond 35:84–99. ISSN 0261-0523. https://doi.org/10.1098/rstl.1883.0029

Schlichting H (1933) Laminare Strahlausbreitung. ZAMM. J Appl Math Mech/Zeitschrift für Angewandte Mathematik und Mechanik 13(4):260–263. ISSN 15214001. https://doi.org/10.1002/zamm.19330130403

Schubauer GB, Skramstad H (1948) Laminar-boundary-layer oscillations and transition on a flat plate. Technical Report 909, National Advisory Committee for Aeronautics, Washington, US. https://ntrs.nasa.gov/search.jsp?R=19930091976

Tollmien W (1928) Über die Entstehung der Turbulenz. 1. Mitteilung. Nachrichten von der Gesellschaft der Wissenschaften zu Göttingen, Mathematisch-Physikalische Klasse, vol 1929, pp 21–44. http://eudml.org/doc/59276